

Hybridized nanocavities as single-polarized plasmonic antennas

Ahmet Ali Yanik,^{1,2} Ronen Adato,^{1,2} Shyamsunder Erramilli,^{1,3} Hatice Altug^{1,2,*}

¹Department of Electrical and Computer Engineering, Boston University, Boston, MA, 02215, USA

²Boston University Photonics Center, Boston, MA, 02215, USA

³Physics Department, and Department of Biomedical Engineering, Boston University, Boston MA, 02215, USA

*altug@bu.edu

Abstract: We experimentally demonstrate that hybridized nanocavities in optically thick metal films radiate in coherence, and act as an efficient single-polarized plasmonic nano-antenna array. We employ propagating and localized plasmons to enhance polarization control along one axis, with total suppression of the perpendicular polarization component. The relationship between the near-field and far-field radiation is established through a quasi-static model connecting the individual nano-antenna behavior to the phenomenon of extraordinary light transmission. Hybridized nanocavity antennas, with length scales below the conventional diffraction limit, present opportunities for potential applications in photovoltaics, optoelectronic devices and optical sensors.

© 2009 Optical Society of America

OCIS codes: (240.6680) Surface plasmons; (250.5403) Plasmonics; (260.3910) Metal optics; (240.5440) Polarization-selective devices

References and links

1. P. J. Schuck, D. P. Fromm, A. Sundaramurthy, G. S. Kino, and W. E. Moerner, "Improving the mismatch between light and nanoscale objects with gold bowtie nanoantennas," *Phys. Rev. Lett.* **94**(1), 017402 (2005).
2. P. Mühlischlegel, H. J. Eisler, O. J. F. Martin, B. Hecht, and D. W. Pohl, "Resonant optical antennas," *Science* **308**(5728), 1607–1609 (2005).
3. E. Cubukcu, E. A. Kort, K. B. Crozier, and F. Capasso, "Plasmonic laser antenna," *Appl. Phys. Lett.* **89**(9), 093120 (2006).
4. R. de Waele, A. F. Koenderink, and A. Polman, "Tunable nanoscale localization of energy on plasmon particle arrays," *Nano Lett.* **7**(7), 2004–2008 (2007).
5. H. F. Raether, *Surface Plasmons on Smooth and Rough Surfaces and on Gratings* (Springer, New York, 1988).
6. S. Maier, *Plasmonics: Fundamentals and Applications* (Springer, New York, 2007).
7. A. Nahata, R. A. Linke, T. Ishi, and K. Ohashi, "Enhanced nonlinear optical conversion from a periodically nanostructured metal film," *Opt. Lett.* **28**(6), 423–425 (2003).
8. S. Kim, J. Jin, Y. J. Kim, I. Y. Park, Y. Kim, and S. W. Kim, "High-harmonic generation by resonant plasmon field enhancement," *Nature* **453**(7196), 757–760 (2008).
9. S. Nie, and S. R. Emory, "Probing Single Molecules and Single Nanoparticles by Surface-Enhanced Raman Scattering," *Science* **275**(5303), 1102–1106 (1997).
10. K. Kneipp, H. Kneipp, I. Itzkan, R. R. Dasari, and M. S. Feld, "Surface-enhanced Raman scattering and biophysics," *J. Phys. Condens. Matter* **14**(18), 597–624 (2002).
11. H. Xu, E. J. Bjerneld, M. Käll, and L. Börjesson, "Spectroscopy of single hemoglobin molecules by surface enhanced Raman scattering," *Phys. Rev. Lett.* **83**(21), 4357–4360 (1999).
12. L. Novotny, "Effective wavelength scaling for optical antennas," *Phys. Rev. Lett.* **98**(26), 266802 (2007).
13. T. W. Ebbesen, H. J. Lezec, H. F. Ghaemi, T. Thio, and P. A. Wolff, "Extraordinary optical transmission through sub-wavelength hole arrays," *Nature* **391**(6668), 667–669 (1998).
14. H. Liu, and P. Lalanne, "Microscopic theory of the extraordinary optical transmission," *Nature* **452**(7188), 728–731 (2008).
15. C. Genet, and T. W. Ebbesen, "Light in tiny holes," *Nature* **445**(7123), 39–46 (2007).
16. W. L. Barnes, A. Dereux, and T. W. Ebbesen, "Surface plasmon subwavelength optics," *Nature* **424**(6950), 824–830 (2003).
17. E. Ozbay, "Plasmonics: Merging Photonics and Electronics at Nanoscale Dimensions," *Science* **311**(5758), 189–193 (2006).
18. L. Martín-Moreno, F. J. García-Vidal, H. J. Lezec, K. M. Pellerin, T. Thio, J. B. Pendry, and T. W. Ebbesen, "Theory of extraordinary optical transmission through subwavelength hole arrays," *Phys. Rev. Lett.* **86**(6), 1114–1117 (2001).

19. P. Lalanne, C. Sauvan, J. P. Hugonin, J. C. Rodier, and P. Chavel, "Perturbative approach for surface plasmon effects on flat interfaces periodically corrugated by subwavelength apertures," *Phys. Rev. B* **68**(12), 125404 (2003).
20. W. L. Barnes, W. A. Murray, J. Dintinger, E. Devaux, and T. W. Ebbesen, "Surface Plasmon Polaritons and Their Role in the Enhanced Transmission of Light through Periodic Arrays of Subwavelength Holes in a Metal Film," *Phys. Rev. Lett.* **92**(10), 107401 (2004).
21. U. Schröter, and D. Heitmann, "Grating couplers for surface plasmons excited on thin films in the Kretschmann-Raether configuration," *Phys. Rev. B* **60**(7), 4992–4999 (1999).
22. J. A. Porto, F. J. Garcia-Vidal, and J. B. Pendry, "Transmission resonances on metallic gratings with very narrow slits," *Phys. Rev. Lett.* **83**(14), 2845–2848 (1999).
23. P. B. Catrysse, and S. Fan, "Propagating plasmonic mode in nanoscale apertures and its implications for extraordinary transmission," *J. Nanophoton.* **2**(1), 021790 (2008).
24. A. M. Dykhne, A. K. Sarychev, and V. M. Shalaev, "Resonant transmission through metal films with fabricated and light-induced modulation," *Phys. Rev. B* **67**(19), 195402 (2003).
25. Y. Ekinici, H. H. Solak, and C. David, "Extraordinary optical transmission in the ultraviolet region through aluminum hole arrays," *Opt. Lett.* **32**(2), 172–174 (2007).
26. R. Gordon, and A. G. Brolo, "Increased cut-off wavelength for a subwavelength hole in a real metal," *Opt. Express* **13**(6), 1933–1938 (2005).
27. W. Fan, S. Zhang, B. Minhas, K. J. Malloy, and S. R. J. Brueck, "Enhanced infrared transmission through subwavelength coaxial metallic arrays," *Phys. Rev. Lett.* **94**(3), 033902 (2005).
28. F. I. Baida, and D. Van Labeke, "Light transmission by subwavelength annular aperture arrays in metallic films," *Opt. Commun.* **209**(1-3), 17–22 (2002).
29. S. M. Orbons, A. Roberts, D. N. Jamieson, M. I. Haftel, C. Schlockermann, D. Freeman, and B. Luther-Davies, "Extraordinary optical transmission with coaxial apertures," *Appl. Phys. Lett.* **90**(25), 251107 (2007).
30. C. Rockstuhl, F. Lederer, C. Etrich, T. Pertsch, and T. Scharf, "Design of an Artificial Three-Dimensional Composite Metamaterial with Magnetic Resonances in the Visible Range of the Electromagnetic Spectrum," *Phys. Rev. Lett.* **99**(1), 017401 (2007).
31. H. J. Lezec, and T. Thio, "Diffracted evanescent wave model for enhanced and suppressed optical transmission through subwavelength hole arrays," *Opt. Express* **12**(16), 3629–3651 (2004).
32. G. Gay, O. Alloschery, B. Viaris de Lesegno, C. O'Dwyer, J. Weiner, and H. J. Lezec, "The optical response of nanostructured surfaces and the composite diffracted evanescent wave model," *Nat. Phys.* **2**(4), 262–267 (2006).
33. S. Lal, S. Link, and N. J. Halas, "Nano-optics from sensing to waveguiding," *Nat. Photonics* **1**(11), 641–648 (2007).
34. E. Prodan, C. Radloff, N. J. Halas, and P. Nordlander, "A hybridization model for the plasmon response of complex nanostructures," *Science* **302**(5644), 419–422 (2003).
35. K. B. Crozier, A. Sundaramurthy, G. S. Kino, and C. F. Quate, "Optical antennas: Resonators for local field enhancement," *J. Appl. Phys.* **94**(7), 4632 (2003).
36. A. Degiron, H. J. Lezec, N. Yamamoto, and T. W. Ebbesen, "Optical transmission properties of a single subwavelength aperture in a real metal," *Opt. Commun.* **239**(1-3), 61–66 (2004).
37. A. A. Yanik, X. Wang, S. Erramilli, M. K. Hong, and H. Altug, "Extraordinary midinfrared transmission of rectangular coaxial nanoaperture arrays," *Appl. Phys. Lett.* **93**(8), 081104 (2008).
38. H. F. Ghaemi, T. Thio, D. E. Grupp, T. W. Ebbesen, and H. J. Lezec, "Surface plasmons enhance optical transmission through sub-wavelength holes," *Phys. Rev. B* **58**(11), 6779–6782 (1998).
39. H. Kuwata, H. Tamaru, K. Esumi, and K. Miyano, "Resonant light scattering from metal nanoparticles: Practical analysis beyond Rayleigh approximation," *Appl. Phys. Lett.* **83**(22), 4625–4627 (2003).

1. Introduction

Antennas play a critical role as transmitters and receivers in radio and microwave communications by efficiently converting propagating electromagnetic fields to localized excitations and vice versa. Likewise, it is highly desirable to focus electromagnetic fields to nanoscale dimensions at visible and infrared frequencies to boost light-matter interactions. With the recent advancements in nanofabrication capabilities, a new generation of antennas operating at the optical and infrared frequencies is rapidly emerging. Plasmonic nanoantenna, with a potential to reshape the photonics field by converting light to sub-wavelength scale localized surface plasmons (LSPs), is at the core of new exciting opportunities [1–6]. Recent studies have demonstrated orders of magnitude enhancement in second harmonic generation [7,8] and in surface-enhance Raman spectroscopy down to the single molecular level [9–11]. Remarkably, many of the well-established concepts for radio and microwave frequencies are shown to be still valid at these small dimensions [12].

The phenomenon of extra-ordinary light transmission (EOT) through the sub-wavelength cavity arrays in optically thick metals films is another example of an interesting physical effect due to the surface plasmons [13–17]. This phenomenon is generally related to the propagating surface plasmon polaritons (SPPs) induced by periodically perturbed metallic

surfaces [14, 18–25]. For periodic perturbations in the form of sub-wavelength openings in a metal film, SPPs propagate along the incidence surface and couple to the out-coupling surface through these openings. Surface plasmons are then converted back to photons on the out-coupling surface and reradiate in the same direction as the incident beam. The EOT characteristics strongly depend on the detailed mechanisms of plasmon coupling between the two surfaces [26–32]. This widely accepted description, on the other hand, clearly separates the concepts of antenna theory and the EOT phenomenon. Likewise, work on optical antennas reported to date has been focused on isolated metallic nanostructures such as nanoparticles, nanoshells, nanorods and bow tie antennas [12,33–35].

In this letter, we introduce a quasi-static model incorporating basic antenna principles similar to those reserved for isolated nano-antennas, and extend it to explain the EOT effect. We show that the complex behavior of EOT in specially designed cavities can be explained in a way that is conceptually similar to the widely known hybridization effects in nanoshells [33]. This approach provides an intuitive picture of EOT, and explains experimentally observed features in complex cavities remarkably well. Our experimental findings demonstrate that periodic nanocavities in optically thick metal films radiate in coherence and act as efficient plasmonic nano-antenna arrays. We also demonstrate that our structures enable enhanced polarization control surpassing the performance of commercially available holographic wire grid polarizers in the mid-infrared region of the spectrum.

2. Concepts and fundamentals

Our studies are based on the rectangular coaxial cavity (RCC) arrays (Fig. 1(a)), which show complex LSP dynamics and SPP mediated EOT effects at the same time. Incident light goes through different electromagnetic states as it travels from the incidence surface to the out-coupling surface. In Fig. 1(b), 3-D FDTD simulations representing the creation, transfer, and out-coupling of surface plasmons are shown for the RCC arrays for polarized light in y -direction. Initially, SPPs are created on the incidence surface at resonance wavelengths

$$\lambda_{SPP} = d / \sqrt{i^2 + j^2} \sqrt{\epsilon_{Si} \epsilon_{Au} / \epsilon_{Si} + \epsilon_{Au}},$$

where the momentum matching condition is satisfied with the set of reciprocal lattice vectors $\vec{G} = i\vec{G}_x + j\vec{G}_y$. Here, d is the lattice constant, and ϵ_{Si} (ϵ_{Au}) is the dielectric constant of the silicon substrate (gold film). At resonance, a symmetric standing wave pattern is apparent in the field profile due to the interference of the counter propagating SPP waves with parallel wavevectors $\pm 2\pi/a$ in the y -direction. Hot spots around the rims of the cavities are due to excitation of LSPs. These localized hot spots scatter the SPPs into attenuated waveguide modes of the subwavelength dimension cavities. In previous studies on periodic arrays, SPP-LSP coupling was not discussed, although the importance of the LSPs for individual cavities was demonstrated by Degiron et al [36]. The generally accepted idea is that LSPs cause only minor changes in EOT characteristics in periodic structures. In the following, we demonstrate that LSPs play an equally important role with SPPs on the EOT effect. We introduce a quasi-static model of EOT effect to analyze the coupling between SPPs and LSPs, and to explain the physical processes involved in direct and SPP mediated transmission of light. At this point, we will leave the details of the SPP-LSP coupling to our quasi-static model discussion below. Instead, we will continue with our FDTD analysis following the LSP scattering of the SPPs to the waveguide modes. As shown in Fig. 1(b), the coupling between the two surfaces of the metal film is mediated primarily by the TE_{01} waveguide mode of the cavity. Finally, on the metal/air interface, waveguide modes are converted directly to out-coupling photons through the LSPs. Contrary to metal/silicon interface, SPP excitations are not allowed at metal/air interface due to the effective index difference causing momentum mismatch. The radiating field pattern in the near-field closely resembles to that of a rectangular aperture waveguide, rather than a dipolar LSP field pattern [37]. There are two important observations in this analysis. First is the presence of LSPs at the rims of the cavities which couple the SPP to the waveguide modes. Second is the preservation of the polarization direction of the electric-field at all electromagnetic states from the creation

of surface plasmons at incident surface to the reradiation of light at the out-coupling surface. These two observations will be used in the development of quasi-static model and the analysis of the transmission strengths of the periodic and individual cavities.

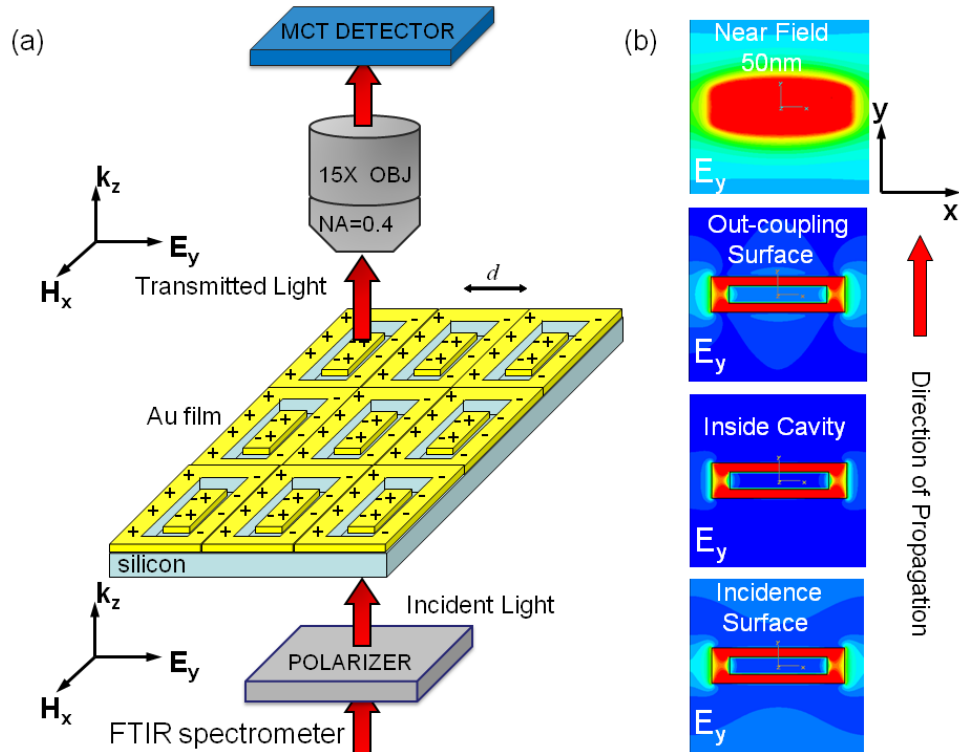


Fig. 1. (a) Experimental measurements are taken in a transmission configuration with light incident from the silicon side. (b) FDTD analysis summarizes the creation, transfer and out-coupling of the plasmons. Propagation direction is indicated by the arrow.

3. Fabrication and optical characterization

A focused-ion-beam system (FIB) is used to mill periodic and random cavity arrays ($\sim 100 \mu\text{m} \times 100 \mu\text{m}$) in a 100 nm thick gold layer evaporated on a silicon substrate with a 5 nm Cr/Ti adhesion layer. As the skin-depth of the gold at the mid-IR part of the spectrum is approximately 10 nm, direct coupling of the plasmons between the two surfaces of the metal film is negligible. The periodic arrays consisting of 50×50 cavities with a period of $a=2 \mu\text{m}$ are fabricated along with arrays consisting of randomly positioned 1500 cavities over an equal total area ($100 \mu\text{m} \times 100 \mu\text{m}$). The openings are $1.5 \mu\text{m} \times 0.4 \mu\text{m}$ for the rectangular cavities (RC) while the RCC have equal dimensions with a coaxial core of $1.1 \mu\text{m} \times 0.2 \mu\text{m}$. A square aperture of $100 \mu\text{m} \times 100 \mu\text{m}$ size (equal to the total array dimensions) is also defined on the same chip to normalize the measured transmitted signal. Randomized arrays of nanorods, identical to the inner core of the RCC, are fabricated on silicon substrates using electron beam lithography and lift-off process. Figure 2 shows scanning electron microscope (SEM) images of the periodic and the randomized nanocavity arrays. Measurements are performed in a transmission configuration using a BrukerTM Fourier-transform infrared (FTIR) spectrometer with a KBr beam splitter (spectral range $350 - 7400 \text{ cm}^{-1}$), connected to an infrared microscope. The light is incident from the silicon substrate side and the transmitted infrared signal is collected with an objective lens ($\text{NA}=0.4$) to a mercury cadmium telluride (MCT) detector (spectral range $600\text{--}12500 \text{ cm}^{-1}$) as shown in Fig. 1(a). Normalized transmissions of the cavity arrays are divided by the air fraction of the gold film to determine the transmissivity. In order to compare periodic and randomized arrays, we

further divided the transmissivity with the number of cavities in each array to estimate the transmissivity per cavity. Similarly, extinction ratios of the nanoparticles are calculated by using normalized transmissions through the nanorod arrays.

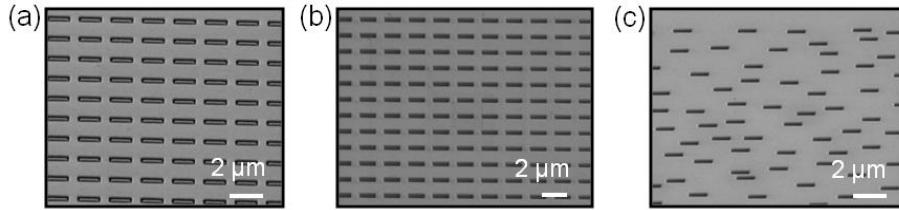


Fig. 2. Scanning electron images of periodic RCC (a) and RC (b) arrays are shown. Randomized RC array (c) are also fabricated to probe LSPs of individual cavities.

Experimentally measured EOT spectra (transmissivity -per cavity- vs wavelength) for the periodic and randomized cavity arrays are shown in Fig. 3. Transmission measurements are performed on randomized arrays in order to probe the LSPs of the individual cavities. Any effects of the periodicity (thus, involvement of SPPs) are canceled through the randomization process and the direct transmission characteristics of the individual cavities are obtained. As show in Fig. 3(a) (solid line), direct transmission spectra have Gaussian shape with no structural Wood's anomalies due to the absence of periodicity [36,38]. Transmission resonances (dashed lines in Fig. 3(a)) are observed at wavelengths $\lambda_{LSP}=9.23 \mu\text{m}$ and $\lambda_{LSP}=10 \mu\text{m}$ for the randomized RC and RCC arrays, respectively. EOT transmissions are higher for individual RCs with respect to individual RCCs for the reasons that will become clear when we discuss the EOT phenomenon in our quasi-static model below. In Fig. 3(a), EOT resonances of the periodic cavity arrays (solid-lines) are observed at $\lambda_{SPP}=7.87 \mu\text{m}$ ($\lambda_{SPP}=8.01 \mu\text{m}$) for the RC (RCC) arrays corresponding to (0,1) grating order at the Au/Si interface. Plasmonic resonance peaks have an asymmetric line-shape close to Wood's anomaly, which occurs approximately at $n_{Si}d$ ($n_{Si}=3.46$ is the refractive index of the substrate). In contrast to previous observations in randomized arrays in periodic arrays, the transmissivities of the RCCs are relatively stronger than that of the RCs. In addition, the transmissivities of the periodic arrays are up to 30 times more efficient than those of randomized arrays. These observations are related to the different excitation mechanisms of the LSPs in randomized and periodic structures, as we discuss below.

The inner cores of the coaxial structures, nanorod antennas, are characterized with extinction measurements obtained from randomized arrays as shown in Fig. 3(b). For incident light polarized along the long axis of the rod (*p*-polarized state), the resonance excitation occurs at $\lambda=6.66 \mu\text{m}$ corresponding to the individual LSP resonances of the nanorods. For *s*-polarized (short axis) incident light, induced dipole strength is much weaker, resulting in lower extinction efficiencies (Fig. 3(b)). However, as we show below, when these nano-rod antennas are placed in a metallic rectangular cavity, they have a profound effect on the strength of the EOT signal even for the *s*-polarized incident light.

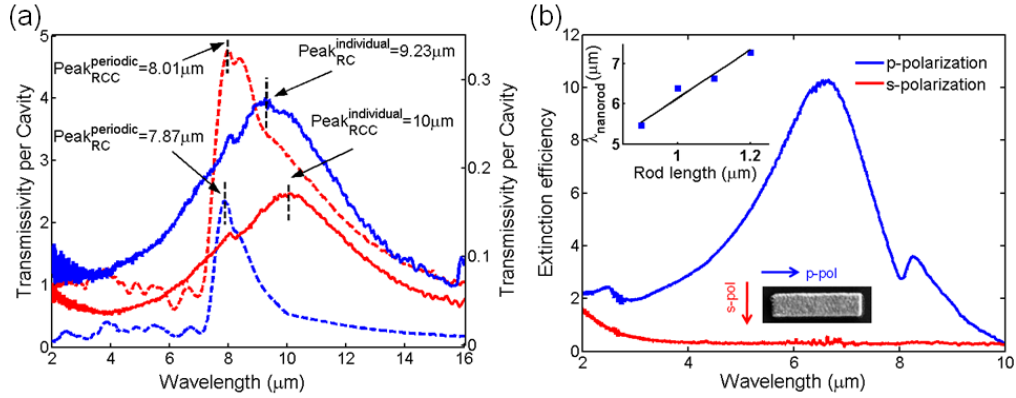


Fig. 3. The transmissivity spectra for the random (solid curves) and periodic (dashed curves) arrays of rectangular (blue) and rectangular coaxial (red) nano-cavities are shown (a). For nanorods, extinction coefficients of s-(red) and p-polarized (blue) light are shown (b). Inset shows the resonance wavelength vs rod length fitted with analytical polarizability. The absorption features observed around 8 μm for p-polarized light are due to the enhanced vibrational absorption of naturally grown SiO₂ film on silicon substrate.

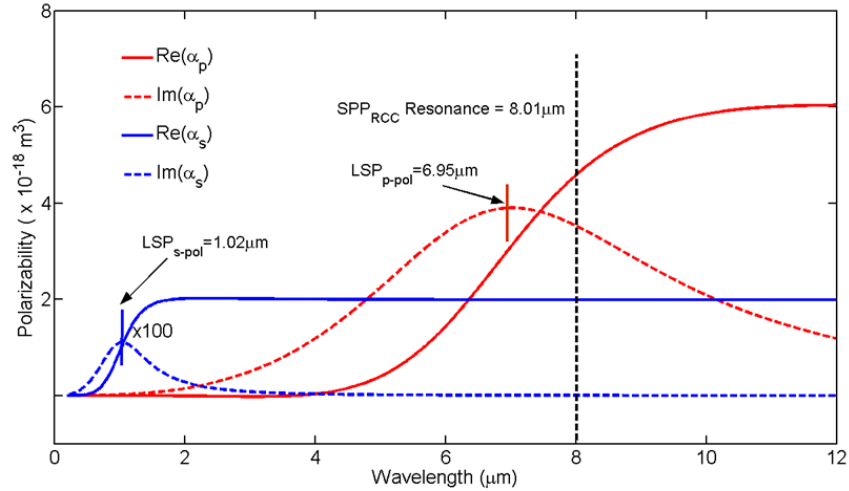


Fig. 4. The polarizability of the individual nanorod antenna is shown in the figure. SPP resonance wavelength/frequency is shown with the black dashed line which is longer/lower than the plasmonic excitation wavelength/frequency in s- and p-polarized states.

Figure 4 shows the real and the imaginary parts of the polarizability (α) of the nanorod antennas for the p- and s-polarized light calculated according to the Kuwata's model [39]. For nanorods with dimensions comparable to the wavelength of light, the Rayleigh approximation is not sufficient due to the large phase delays within the driving field over the particle volume. Instead, Kuwata *et al* has formulated an empirical extension of the Mie's theory for rod-like structures:

$$\alpha_{s,p} \approx \frac{V}{\left(L_{s,p} + \frac{\epsilon_d}{\epsilon_m - \epsilon_d} \right) + A\epsilon_d x^2 + B\epsilon_d^2 x^4 - i \frac{4\pi^2 \epsilon_d^{3/2} V}{3 \lambda^3}} \quad (1)$$

where, V is the volume of the particle, ϵ_d and ϵ_m represents the dielectric constants of the medium and metal antenna, respectively. $L_{s,p}$ is the depolarization factor in s-/p-polarization

and $x = \pi a / \lambda$ is the size parameter, a being the length of the antenna. A and B are geometrical factors that have been defined as [39]: $A = -0.4865L_{s,p} - 1.046L_{s,p}^2 + 0.8481L_{s,p}^3$, and $B = 0.01909L_{s,p} + 0.1999L_{s,p}^2 + 0.6077L_{s,p}^3$. For a nanorod modeled as a cylinder capped with hemispheres, the geometrical factors for the p-polarized light is calculated to be $L_p = e^{-1} - 2 - e^2 - 2e - 1 \sqrt{e^2 - 2e + 2} / 3 e^{-1}^3$, and $2 \times L_s + L_p = 1$, where $e = a/b$ is the aspect ratio. The real and imaginary parts of the polarizability represent the radiation amplitude and the radiation phase, respectively. Nanorod polarizability for the p-polarized light, calculated to be at $\lambda_{nanorod} = 6.95 \mu m$, is more than two orders of magnitude larger than that for the s-polarized light. Accordingly, s-polarized plasmonic resonances of the nanorods, which is predicted to be at $\lambda = 1.02 \mu m$ (Fig. 4) are not observable in our experiments (Fig. 3(b)). As can be deduced from Eq. (1), the dipole moment of the metallic nanorods undergoes a change of sign, when the structural resonance frequency is crossed at the critical point where the sign of the denominator changes (Fig. (4)). For a s-polarized external field driving the system at a frequency ($\lambda_{SPP} = 8.01 \mu m$ indicated with vertical dashed line in Fig. 3(a)) lower than the structural resonance frequency of the nanorod antenna ($\lambda_{nanorod} = 1.02 \mu m$ in Fig. (4)), the induced nanorod dipole is in phase with the external field. Here the charge oscillations can easily follow the driving field.

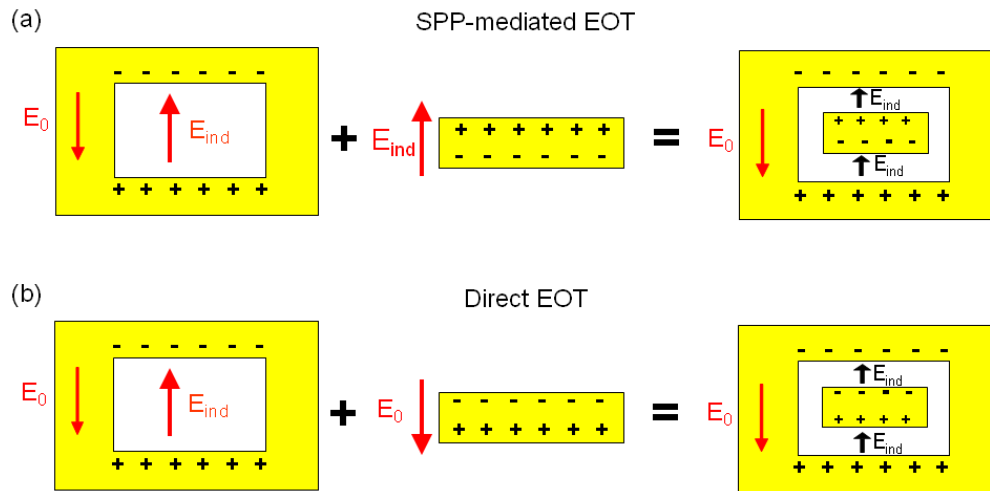


Fig. 5. Quasi-static model of EOT effect for rectangular coaxial cavities is shown for (a) SPP-mediated and (b) direct coupling of light to LSPs.

The LSP characteristics of a cavity can as well be expressed with a dipole moment $p = \alpha E$, where α is the polarizability of a dielectric void embedded in a metallic medium. Unlike nanorods, rectangular cavity polarizabilities, however, cannot be readily obtained using analytical means. One way to determine the phase factor of the nano-cavity polarizability is to find out the EOT resonance wavelength of the individual cavities. As shown in Fig. 3(a), the resonance frequency dictated by the periodicity ($\lambda_{SPP} = 8.01 \mu m$) is higher than the resonance frequency of the individual rectangular cavities ($\lambda_{LSP} = 9.23 \mu m$). Accordingly, electric charges accumulated inside the cavity surfaces are arranged in a way that the induced electric field is in the opposite direction to the external electric field at $\lambda_{SPP} = 8.01 \mu m$, as shown in Fig. 5(a).

4. Quasi-static model

Our quasi-static model is based on the two critical observations outlined in our FDTD analysis. The LSPs in the cavity rims serve as electric dipoles, which scatter the light coupled

either through the SPPs or directly from the continuum. Preservation of the polarization direction of the E-field component through all the interfaces and inside the cavities enables us to define a net dipole moment for the LSP scattering into the waveguide modes. Within this model, LSPs in cavities with complex shapes such as RCC can be understood through the hybridization of the plasmons supported by the rectangular cavities and nano-rods/inner-core (Fig. 5(a)). The effective dipole moment of an individual RCC in an array can be written as:

$$\vec{p}_{RCC} = \alpha_C \vec{E}_0 + \vec{E}_{core} = \alpha_C \vec{E}_0 + \alpha_C \tau_{cav-rod} \alpha_R \vec{E}_{ind} \quad (2)$$

where the net electric field acting on the cavity is the incident field \vec{E}_0 plus the inner core field $\vec{E}_{core} = \tau_{cav-rod} \alpha_R \vec{E}_{ind}$ due to the induced charges on the rod. α_C and α_R are the polarizabilities of the cavity and the nanorod, respectively at the resonance frequency of the SPP (dashed line in Fig. 4). $\tau_{cav-rod}$ is the coupling parameter relating the induced dipole moment of the inner core $\vec{p}_R = \alpha_R \vec{E}_{ind}$ to the effective field \vec{E}_{core} of the inner core acting on the cavity. The induced dipole moment of the cavity is proportional to the electric field inside the cavity $\vec{E}_{ind} = \kappa \vec{p}_{RCC}$, where κ is a negative geometrical factor. The net electric dipole moment of the coaxial cavity can then be simplified to $\vec{p}_{RCC} = \alpha_C \vec{E}_0 / (1 - \alpha_C \alpha_R \tau_{cav-rod} \kappa)$. At the SPP resonance of the periodic pattern ($\lambda_{SPP} = 8.01 \mu\text{m}$), the structural polarizabilities α_C and α_R of the cavity and the inner core are positive, while coupling parameter $\tau_{cav-rod}$ is always a negative quantity. Accordingly, the denominator of the \vec{p}_{RCC} is less than one. The stronger dipole moment for the RCC arrays ($\vec{p}_{RCC} > \vec{p}_{RC} = \alpha_C \vec{E}_0$) causes a larger induced electric field inside the cavity openings. Induced charges in the inner/outer surfaces of the cavities/cores of the RCC squeeze the electromagnetic field into a smaller volume in agreement with our FDTD calculations (Fig. 6). This leads to an enhanced coupling between SPPs and waveguide modes causing stronger transmissions for the periodic RCC arrays as observed in our experimental measurements (dashed curves in Fig. 3a).

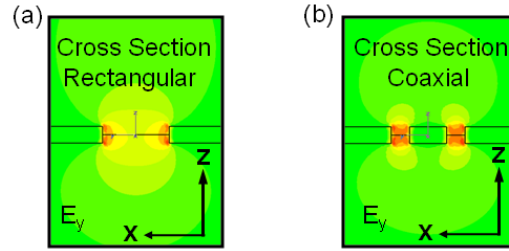


Fig. 6. (a) Cross sectional image of the rectangular cavity is shown at the SPP resonance frequency. (b) FDTD analysis shows the enhancement of the field inside the coaxial-cavity due to the hybridization with respect to simple rectangular cavity.

In the case of direct coupling of incident light to the randomized cavities, the field acting on the inner core is the external field \vec{E}_0 . Accordingly, the dipole moment of the inner core is proportional with the external electric field and in-phase with it (Fig. 5(b)). In this case, the effective dipole moment of an individual RCC can be written as:

$$\vec{p}_{RCC} = \alpha_C \vec{E}_0 + \alpha_C \tau_{cav-rod} \alpha_R \vec{E}_0 \quad (3)$$

At the SPP resonance of the periodic pattern ($\lambda_{SSP} = 8.01 \mu\text{m}$), the structural polarizability α_R of the inner core is positive. Accordingly, the net dipole moment of the RCC ($\vec{p}_{RCC} = \alpha_C 1 + \alpha_R \tau_{cav-rod} \vec{E}_0$) is smaller than the dipole moment of the RC ($\vec{p}_{RC} = \alpha_C \vec{E}_0$) independently from the cavity polarizability α_c . Induced charges in the inner surfaces of the cavity and the outer rims of the core counteract each other's electric fields resulting in a smaller net dipole moment (Fig. 5(b)). This is in agreement with experimental measurements showing that EOTs are less efficient for the randomized RCC arrays with respect to RCs (solid curves in Fig. 3(a)).

5. Hybridization of plasmonic excitations

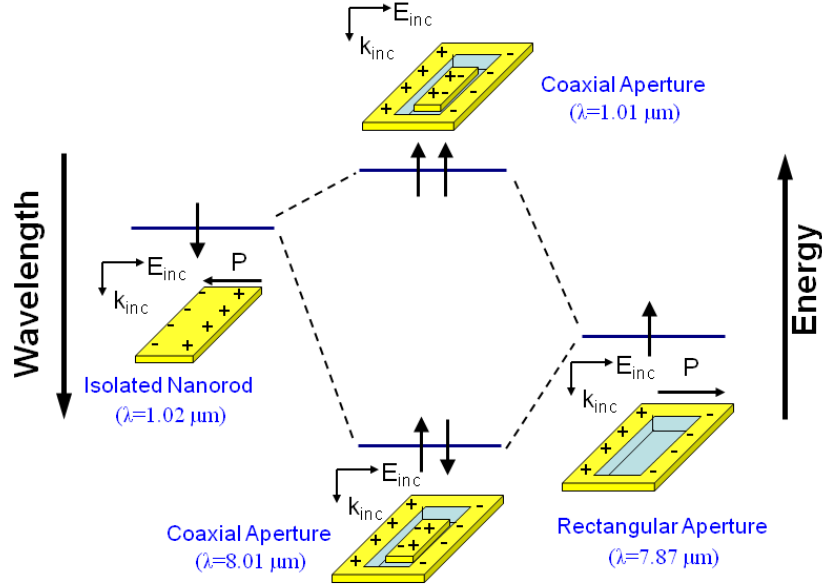


Fig. 7. Hybridization model for experimentally observed red-shift is shown for RCC as a result of interaction between the rectangular nano-cavity and inner core. Energy splitting results in red shifting of the rectangular coaxial aperture resonances.

As explained above, the presence of the inner core increases the coupling efficiency between the SPPs and the waveguide modes, resulting in higher transmissivities for periodic RCC arrays. This coupling also leads to a red shifting of the transmission maximum (Fig. 3(a)), which can be described by the hybridization of the two elementary plasmonic excitations as shown in Fig. 7. The plasmonic hybridization picture completes the nano-antenna approach we develop above, while describing the sensitive structural tunability of the plasmonic resonance wavelengths. A similar hybridization scheme has been utilized for isolated complex nano-shell antenna [33]. The Hamiltonian of the coaxial rectangular aperture, with an interaction coupling term V_{int} , can be written as,

$$H = H_{cavity} + H_{rod} + V_{int} = \begin{bmatrix} \epsilon_{cavity} & \Delta \\ \Delta^* & \epsilon_{rod} \end{bmatrix} \quad (4)$$

where, $\epsilon_{cavity} = 0.158 \text{ eV } \lambda = 7.83 \mu\text{m}$ and $\epsilon_{rod} = 1.216 \text{ eV } \lambda = 1.02 \mu\text{m}$ are the excitation energies for the cavity and the inner core for the *s*-polarized light while $\Delta = 55 \text{ meV}$ is an empirical coupling term. This coupling causes splitting of the plasmon resonances into lower energy “bonding” $\epsilon_b = 0.155 \text{ eV } \lambda = 8.01 \mu\text{m}$ and higher energy “anti-bonding”

$\varepsilon_b = 1.218 eV$ $\lambda = 1.01 \mu m$ states as in molecular orbital theory. Here, the bonding plasmonic excitation is anti-symmetric while the anti-bonding excitation is symmetric, unlike previous observations in nano-shell structures [34]. This phenomenon is unique to the coaxial cavities in metallic films and opens up new opportunities for fine LSP tuning in EOT phenomenon.

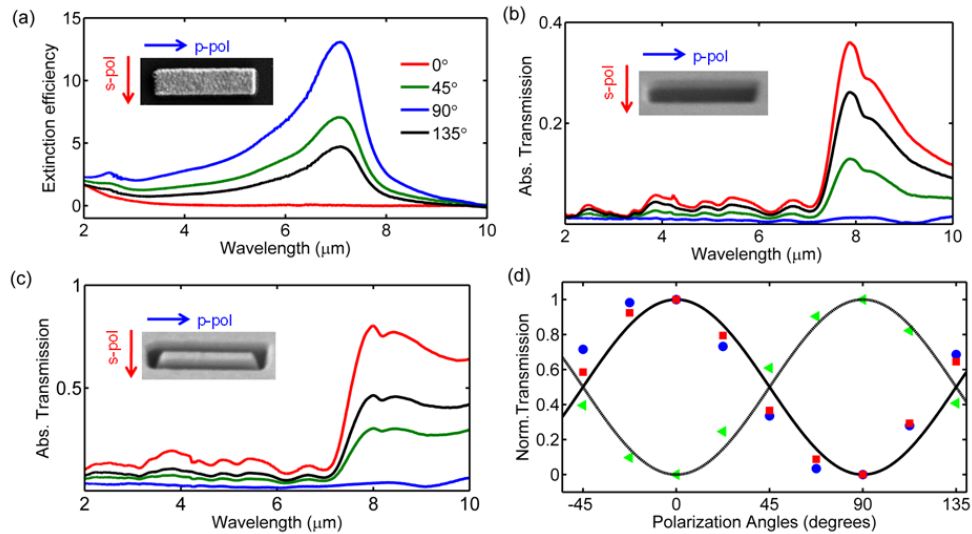


Fig. 8. (a) Extinction efficiency for Nanorod antennas is given for changing polarization angles for incident light. Polarization dependence of the EOT signal is shown for (b) rectangular and (c) coaxial nano-cavities. Complementary behavior of the RCC (red square) and RC (blue circles) cavities and the nanorods (green triangles) are observed.

6. Polarization control

Figure 8(b) and Fig. 8(c) present the transmissivity of RCC and RC arrays for different polarization directions. The EOT spectra are clearly affected by the incident light polarization, as the strength of the LSPs and light scattering to the waveguide modes are controlled by the polarizability of the cavities. Incident light with *s*-polarization (along the short axis of the cavities) is transmitted two orders of magnitude more efficiently than the *p*-polarized light for a cavity with an aspect ratio of only $\sim e = a/b = 4$. This behavior is reversed in the case of nano-rods, where the extinction is maximum when the LSPs are excited along the long axis of the antennas (Fig. 8(a)). Figure 8(d) shows the classical Malus law for polarization dependence of the EOT strength and the extinction efficiency. The signals are normalized to unity with the maximum transmission/extinction of the incident light, while their minimum is set as background. EOT strength of the cavities and the extinction efficiencies of the nanorods follows a complementary behavior, in accordance with Babinet's principle (Fig. 8(d)).

7. Conclusion

In conclusion, we demonstrated that EOT effect and nano-antenna behavior are strongly interrelated. We showed that periodic nanocavities in optically thick metal films radiate in coherence and act as an efficient plasmonic nano-antenna. We also showed that well known nano-antenna phenomena such as hybridization effects are observable in EOT structures. We introduced a quasi-static model for SPP-LSP coupling which can explain experimental measurements remarkably well. We demonstrated that different excitation mechanisms of the LSPs are responsible for the inverse signal strength dependence of the randomized and periodic cavity arrays. Our findings shows that LSPs in periodic RCC arrays can be utilized

for enhanced polarization control, surpassing commercially available holographic grid polarizers.

Acknowledgments

This work is supported in part by NSF SGER Award (Grant No. ECCS-0849603), Massachusetts Life Science Center New Investigator Award, NSF funded Engineering Research Center on Smart Lighting, Boston University College of Engineering Dean's Catalyst Award, Boston University Photonics Center and Army Research Laboratory.